Plasma Jets Driven by Ultraintense-Laser Interaction with Thin Foils

Kar, S., Borghesi, M., Bulanov, S. V., Key, M. H., Liseykina, T. V., Macchi, A., Mackinnon, A. J., Patel, P. K., Romagnani, L., Schiavi, A., & Willi, O. (2008). Plasma Jets Driven by Ultraintense-Laser Interaction with Thin Foils. *Physical Review Letters*, *100*(22), [225004]. https://doi.org/10.1103/PhysRevLett.100.225004

Published in:
Physical Review Letters

Document Version:
Publisher's PDF, also known as Version of record

Plasma Jets Driven by Ultraintense-Laser Interaction with Thin Foils

S. Kar,[1,*] M. Borghesi,[1] S. V. Bulanov,[2] M. H. Key,[3] T. V. Liseykina,[4] A. Macchi,[5] A. J. Mackinnon,[3] P. K. Patel,[3] L. Romagnani,[1] A. Schiavi,[6] and O. Willi[7]

[1]*School of Mathematics and Physics, Queen's University, Belfast, BT7 1NN, United Kingdom*
[2]*APRC, JAEA, Kizugawa, Kyoto 6129-0215, Japan*
[3]*Lawrence Livermore National Laboratory, Livermore California 94550, USA*
[4]*ICT, SB-RAS, Novosibirsk, Russia and MPI-K, Heidelberg, Germany*
[5]*polyLAB, CNR-INFM and Physics Department, University of Pisa, Pisa, Italy*
[6]*Dipartimento di Energetica, Università di Roma 1 "La Sapienza," Roma, Italy*
[7]*Institut für Laser-und Plasmaphysik, Heinrich-Heine-Universität, Düsseldorf, Germany*

(Received 28 August 2007; published 4 June 2008)

Experimental evidence of plasma jets ejected from the rear side of thin solid targets irradiated by ultraintense ($>10^{19}$ W cm^{-2}) laser pulses is presented. The jets, detected by transverse interferometric measurements with high spatial and temporal resolutions, show collimated expansion lasting for several hundreds of picoseconds and have substantially steep density gradients at their periphery. The role played by radiation pressure of the laser in the jet formation process is highlighted analytically and by extensive two-dimensional particle-in-cell simulations.

DOI: 10.1103/PhysRevLett.100.225004 PACS numbers: 52.38.Kd, 41.75.Jv, 52.27.Ny

Interaction of currently available laser pulses at intensity exceeding 10^{20} W cm^{-2} with dense matter leads to extreme conditions [1]. The radiation pressure of these pulses is so high that significant ponderomotive action on the irradiated target is expected despite their relatively short duration (typically of ps order) [2,3]. Ion acceleration is a key application of ultraintense laser-matter interaction [4,5]. Most of the experimental results obtained so far have been explained in the framework of the target normal sheath acceleration (TNSA) mechanism [6,7], where the energy transfer from the laser to ions located at the target rear surface is mediated by electrons. However, several theoretical works have discussed acceleration driven ponderomotively at the target surface [8] or by shocks launched into the target [9,10]. The piston effect of ultraintense ($>10^{23}$ W cm^{-2}) laser radiation pressure has been recently discussed in a numerical and theoretical study [11] showing a cocoonlike deformation of ultrathin foils and acceleration of the ions up to relativistic velocities in the forward direction. A transition to the radiation pressure regime at more moderate intensities has been recently identified via multiparametric particle-in-cell (PIC) simulations [12]. Although without reaching the dramatic effects observed in [11], at lower irradiances one can still expect that the forward momentum transfer from laser to the target ions [12] may result in collimated plasma ejection from the rear of thin foil targets. In this Letter we show the experimental evidence of quasicollimated plasma jet formation at the rear side of thin (few μm) foils irradiated by intense (10^{19}–10^{20} W cm^{-2}) laser pulses. The expansion of the jets was observed lasting for several hundreds of picoseconds (ps). The underlying physical mechanism was studied by employing two-dimensional (2D) PIC simulations. On the basis of these numerical results and of analytical considerations, we suggest that the radiation pressure of the laser has a dominant role in the plasma jet formation process.

The data were collected from two experimental campaigns (say, expt-1 and expt-2) employing VULCAN Nd-glass laser of Rutherford Appleton Laboratory, U.K., operating in chirped pulse amplification (CPA) mode. In expt-1(expt-2), the CPA pulse delivered 60 J (250 J) of energy in 1 ps (0.7 ps) duration. Employing an $f/4.5$ ($f/3$) off-axis parabola the beam was focused down to a 12 μm (5 μm) full width at half maximum (FWHM) spot over the foil target, achieving a peak intensity 3×10^{19} W cm^{-2} (2×10^{20} W cm^{-2}). The CPA pulse was preceded by a low-intensity [$\sim 10^{-6}$ ($\sim 10^{-7}$) times the peak intensity] amplified spontaneous emission (ASE) pedestal about 500 ps (2 ns) long. The targets used in the experiments were free standing thin foils of various materials and thicknesses. A Nomarsky modified interferometer [13] was employed in order to probe transversely the plasma density at both sides of the laser irradiated target. The probe beam was a 527 nm wavelength low-intensity laser beam, achieved by frequency doubling a part of the main CPA pulse. The plasma was probed at different times with temporal resolution equal to the pulse duration of the probe beam. The spatial resolution of the interferometer was a few μm. Reconstruction of the plasma density profile from the interferogram was obtained by retrieving the phase map, by 1D fast Fourier transform of the fringe pattern, followed by *Abel* inversion process assuming a cylindrical symmetry [14].

In expt-1, the interaction of the CPA with a 3 μm thick Al foil was probed transversely at various times, starting from 0 to 250 ps after the arrival of the CPA on the target. A small plasma bulging out from the rear side of the foil was observed at early probing times [up to 40 ps after the arrival of CPA]. At later times the plasma on the rear side of the target was observed expanding in a collimated fashion. The

latest observation was at 250 ps after the arrival of CPA, as shown in Fig. 1(a). Similarly in expt-2, the presence of a long collimated plasma jet was detected at the rear side of a 5 μm thick Cu foil [see Fig. 1(c)], which was probed at 400 ps after the CPA interaction with the target. The region where no fringes were observed in the interferograms corresponds to the shadow of the target, typically having a small amount of transverse tilt due to imperfect flatness of the foil. Nevertheless, the strong second harmonic self-emission from the target enabled us to locate the precise location of the interaction point within the shadow. Fringes in the interferograms move to the left in the presence of the plasma, except the rear side of the target in Fig. 1(a) where they move to the right. A Nomarsky interferogram typically provides two equivalent images displaced side by side, and the fringe displacement in the presence of a plasma is to the left (right) in the left-end (right-end) image [13]. While Fig. 1(b) is the left-end image of the Nomarsky interferogram, in Fig. 1(a) the front plasma is taken from the left-end image and the rear plasma from the right-end image.

As suggested by the data obtained for thicker targets in both the experiments, a key factor to produce a sustained plasma jet appears to be the thickness of the target. Figures 2(a) and 2(b) show, respectively, the interferogram and the electron density profile of the plasma, at the rear side of a 20 μm Cu foil, observed at 400 ps after the interaction in expt-2. The distinctive feature of the plasma jet, i.e., the steep density gradient at their periphery (as typically observed for thinner targets shown in Fig. 1) is clearly absent in this case [see Fig. 2(c)]. In this case, roughly 4 times lower density (2.5×10^{18} cm^{-3} at $z \sim$ 400 μm) plasma is observed with a much larger longitudinal density scale length, compared to the case of 5 μm thick Cu foil shown in Fig. 1(d).

From the data obtained at different probing times (from 50 to 250 ps after the arrival of interaction CPA on target) longitudinal (along CPA axis) and transverse velocities of the jet were estimated. For the case of 3 μm Al foil in expt-1, the longitudinal velocity of the expanding plasma jet is found to be $2 \pm 1 \times 10^6$ m/s. In this case the transverse expansion velocity of the plasma jets is estimated as $6 \pm 2 \times 10^5$ m/s, a significant (3–4) factor lower than the longitudinal velocity. Similarly, from the data collected in expt-2, shown as Fig. 1(d), the longitudinal and transverse expansion velocity of the jet can be measured as 1×10^6 m/s and $4 \pm 1 \times 10^5$ m/s, respectively.

The characteristics of the observed jets rule out the possibility of TNSA mechanism causing their appearance. In the same experiments, acceleration of protons up to tens of MeV was seen, while the velocity of the jets implies ion energies of $\sim$10 keV/nucleon. A general feature of the TNSA mechanism is that the low energy ion component has large source size and high divergence [15,16]. Considering, for example, the $\sim$150 μm source size and

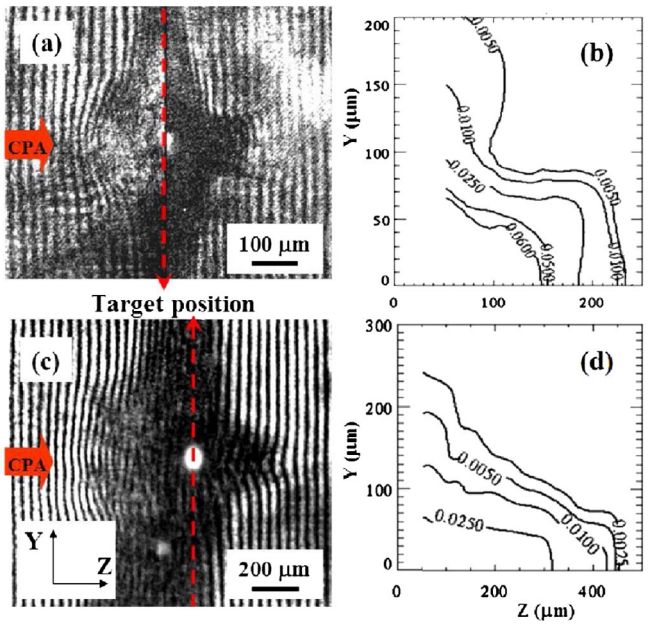

FIG. 1 (color online). Interferograms obtained at (a) expt-1 and (c) expt-2 for 3 μm Al and 5 μm Cu foil targets, respectively. The interferograms were taken at 250 and 400 ps, respectively, after the arrival of the CPA on target. Spatial scales shown in the images correspond to the scales in the object plane. The inverted electron density profile contour plots (in the unit of 10^{21} cm^{-3}) of the rear side plasma are shown next to the respective intergerograms [(b),(d)]. $(Y, Z) = (0, 0)$ corresponds to the point of CPA interaction with the target.

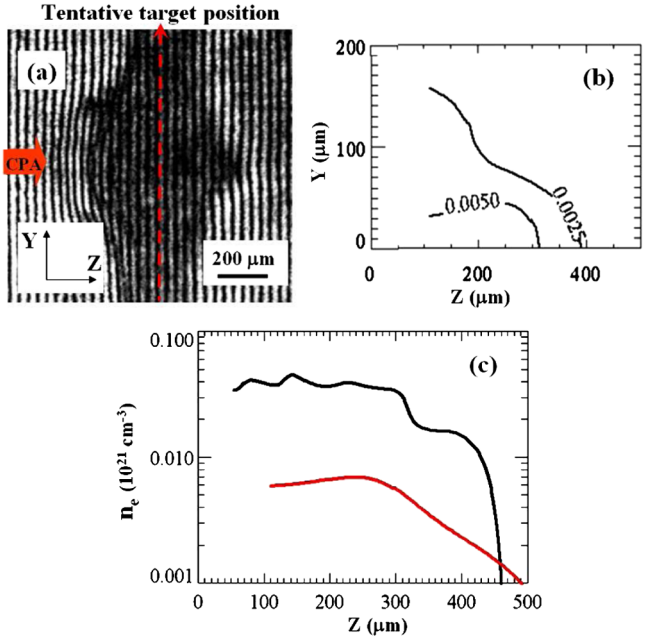

FIG. 2 (color online). (a) Interferogram taken at 400 ps after the arrival of CPA on 20 μm Cu foil in expt-2. The spatial scale mentioned in the image corresponds to the scale in object plane. (b) The inverted electron density profile contour plots (in the unit of 10^{21} cm^{-3}) of the rear side plasma obtained from the interferogram. (c) Comparison between the on-axis electron density profile shown in (b) (red or gray) and Fig. 1(d) (black).

30° divergence reported for 1 MeV/nucleon ions (velocity $\sim 10^7$ m/s) in [16], one would expect that much slower ions accelerated via this mechanism would come from a much larger source than observed. In fact, recent studies of petawatt laser interactions show TNSA-accelerated low energy ions are being emitted from the entire rear surface of mm scale targets [17].

In order to explain the observed longitudinal velocity achieved by the plasma jet, we considered a *piston*-like push of the portion of the target that has been irradiated by the laser pulse. Within the framework of the one-dimensional snowplow approximation, we can write the equation of motion of the plasma (in nonrelativistic approximation) as $\frac{d}{dt}[N(x)\frac{dx}{dt}] = E_0^2/2\pi m_i$, where $N(x) = \int_0^x n_{\text{foil}}(s)ds$ with $n_{\text{foil}}(x)$ being the ion density distribution inside the foil, E_0 is the laser electric field, and m_i is the ion mass. Assuming the duration of the incident short pulse is sufficient to displace the foil by its thickness, i.e., for $\tau_{\text{laser}} > l_{\text{foil}}/\Delta v$, where l_{foil} and Δv are the foil thickness and the ion velocity, we obtain $\Delta v = E_0/\sqrt{2\pi n_{\text{foil}} m_i}$. Let us introduce a dimensionless parameter $b \equiv \Delta v/c = \sqrt{2a_0^2 n_c Z m_e/n_{\text{foil}} m_i}$, ($a_0$ is the laser strength parameter) which characterizes the ion acceleration regime, and $w = E_0^2 \tau_{\text{laser}}/4\pi n_{\text{foil}} l_{\text{foil}} m_i c = b^2 l_{\text{laser}}/2l_{\text{foil}}$. The efficiency of the laser energy transformation into the kinetic energy of fast ions is $\eta = \varepsilon_{i,\text{kinetic}}/\varepsilon_{\text{laser}} = (\Delta v/c)^2$. For $\tau_{\text{laser}} > l_{\text{foil}}/\Delta v$, the ion kinetic energy is given by Eq. (17) in Ref. [18]. In the nonrelativistic limit when $w \ll 1$, $\varepsilon_{i,\text{kinetic}} \approx 2m_i c^2 w^2$ and $\eta \approx 2w$. The ion acceleration mechanism corresponds to the radiation dominant regime. On the other hand, in the case of thick enough targets, i.e., when $\tau_{\text{laser}} < l_{\text{foil}}/\Delta v$, this is the so-called *collisionless shock acceleration* at the front side of the target as analyzed in Refs. [10,19,20].

According to the above expressions, the axial velocity of the jet emerging from a displaced Al foil ($n_{\text{foil}} \approx 60 n_c$) at a laser irradiance of 3×10^{19} W/cm^2 (i.e., $a_0 = 4.7$) will be 1.5×10^6 m/s. Similarly, the longitudinal velocity of the plasma jet from the rear side of a Cu foil ($n_{\text{foil}} \approx 85 n_c$) irradiated at 10^{20} W/cm^2 ($a_0 = 8.5$) will be in the range $1–2 \times 10^6$ m/s, in broad agreement with the experimental observations discussed above. Based on the simple one-dimensional analytical treatment, the thickness of the targets used when the jets are observed (a few μm) sits approximately on the threshold between the two acceleration regimes discussed above ($\Delta v \times \tau_{\text{laser}}/l_{\text{foil}} \sim 0.7$ and 0.2 for the data collected in expt-1 and expt-2, respectively). This corresponds to an intermediate situation in which the piston push may not lead to whole target acceleration, but the ponderomotively pushed ions at the front surface can easily be transported through the thin target resulting in the jetlike expansion at the rear. In the experiment one should also consider that the prepulse erosion may reduce the thickness of undamaged solid density target present at the peak of the CPA pulse. On the contrary, in the case of Fig. 3(a), i.e., where the jet is not observed, the thickness of the target requires at least an order of magnitude longer CPA pulse used in the experiment for approaching the requirements for whole target acceleration. Furthermore, collisional stopping of ions pushed at the front surface as they propagate through the target is likely to play a role in preventing their emergence as a jet at the target rear if the target is thick enough.

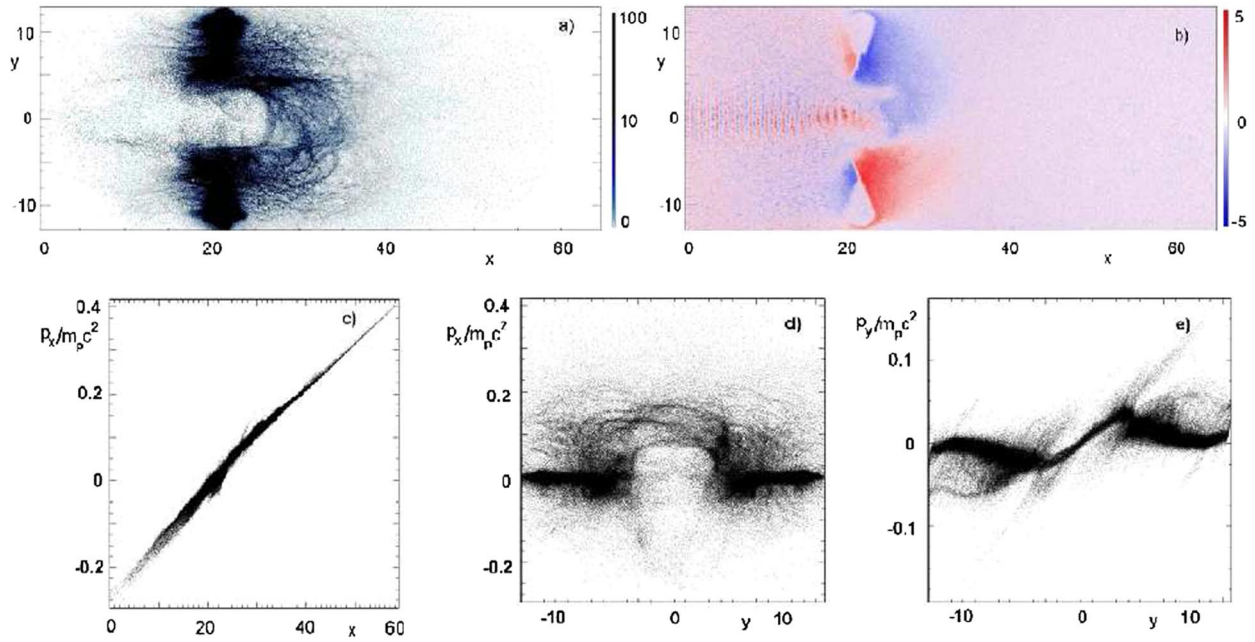

FIG. 3 (color online). Results obtained from 2D PIC simulation. (a) Ion density distribution in the x, y plane at $t = 1.7$ ps; (b) the z component of the magnetic field distribution in the x, y plane at $t = 1.35$ ps. Phase plane view graphs for (c) (Px, x), (d) (Px, y), and (e) (Py, y) at $t = 1.2$ ps.

Some further considerations can be made regarding the role played by the prepulse. The observation of energetic protons in both experiments implies that the prepulse was not capable of eroding the total target thickness before the arrival of the main CPA on target [21]. Indeed, 2D hydrodynamic simulations using the code POLLUX [22] indicate that ablation by a prepulse with the experimental parameters is not sufficient to disrupt the rear surface of foils thicker than 1 μm. A combination of the hydrosimulation results and interferometric measurements also provides information on the plasma conditions at the front surface immediately before the CPA interaction: the preplasma has a gradient of a few μm scale length at the critical density surface, which is located a few μm in front of the solid density target.

In order to support the considerations discussed above, we performed model PIC simulations of the interaction. A full scale PIC simulations of the jet dynamics over the time scales of the experimental observations cannot be accomplished by presently available computational power. However, a clear understanding of the radiation pressure effect of the intense laser pulse interaction with a thin overdense plasma slab is highly pedagogical. By employing the 2D version of the REMP [23] code we simulate the initial stage of the plasma jet formation over a time interval which is finite but substantially longer than the laser pulse duration. In the numerical simulations, a p-polarized laser pulse interacts with an overdense plasma slab in a computation box of size $125\lambda \times 30\lambda$. The pulse is Gaussian, with effective sizes of $250\lambda \times 7\lambda$ and the amplitude $a_0 = 3$. This amplitude value corresponds to a pulse intensity of 1.23×10^{19} W/cm^2 at the wavelength, $\lambda = 1$ μm, in which case the dimensionless parameter b and w are equal to 10^{-2} and 4.2×10^{-3}, respectively. The thickness of the foil is taken as equal to 3λ and its density as $25n_c$. The ratio Zm_e/m_i is equal to 1.361×10^{-4}, which corresponds to the effective ionization (mean ion charge) $Z = 6.745$ for the Al foil and $Z = 15.9$ for Cu target. The front side of the foil interacting with a laser pulse becomes deformed and the ions are accelerated in the forward direction under the action of the laser pulse ponderomotive force [see Fig. 3(a)]. The plasma flow at the target rear side extends over for 25 μm in 1.7 ps. The longitudinal ion momentum is several times larger than the transverse momentum [see Figs. 3(c)–3(e)], and the ion-electron cloud propagates in the forward direction in a form of a collimated bunch. The longitudinal ion momentum and their velocity, $\Delta v \approx 5 \times 10^{-3}c$, correspond to $b = 5 \times 10^{-3}$. The transverse velocity is approximately 4 times lower. In separate simulations we verified that a preplasma as present, for example, in Expt-1, i.e., having a near critical scale length of $\sim$5 μm, has no effect on the jet formation process. In fact, simulations show that ponderomotive steepening of the density profile near critical takes place as the intensity rises on target, and at the peak of the pulse the ponderomotive pressure is directly exerted on the bulk target density.

An additional collimation effect comes from the quasistatic magnetic field generated by fast electrons at the rear side of the target. The magnetic field with its maximal strength $B \approx 5m_e\omega_0 c/e$ at $t = 1.35$ ps [see Fig. 3(b)] by acting on the electrons pinches the plasma jet towards the axis. The bunch transverse size is approximately equal to the waist of the irradiated region, $\approx$10 μm. The magnetic field can contribute significantly to the long term pinching of the ejected plasma plumes [24]. Since the ion momentum distribution along the x direction shown in Figs. 3(c)–3(e) is laminar there will no ion momentum isotropization and one should expect the jet persistence at later times. As a result of the jet ballistic motion after 250 ps its length and width will reach approximately 400 and 100 μm, respectively, in agreement with the experimental measurement.

In conclusion, collimated plasma expansion from the rear side of thin targets irradiated with high power lasers has been observed in different experimental conditions. The thickness of the target is seen to play a vital role for the jet formation from the rear side. From the basis of the 2D simulations and 1D snowplow model the mechanism of the collimated jet formation is consistent with the effect of the strong radiation pressure of laser on thin solid targets.

The data have been collected in experiments supported by RAL and LLNL team. The authors acknowledge financial support from QUB IRCEP, Royal Society, EPSRC, DFG No. TR18, GK 1203, special coordination funds for promoting science and technology commissioned by MEXT of Japan, and the MIUR (Italy) via a PRIN project.

*s.kar@qub.ac.uk

[1] G. A. Mourou *et al.*, Rev. Mod. Phys. **78**, 309 (2006).
[2] S. Wilks *et al.*, Phys. Rev. Lett. **69**, 1383 (1992).
[3] B. Dromey *et al.*, Phys. Rev. Lett. **99**, 085001 (2007).
[4] L. Robson *et al.*, Nature Phys. **3**, 58 (2007).
[5] M. Borghesi *et al.*, Fusion Sci. Technol. **49**, 412 (2006), and references therein.
[6] S. P. Hatchett *et al.*, Phys. Plasmas **7**, 2076 (2000).
[7] P. Mora, Phys. Rev. Lett. **90**, 185002 (2003).
[8] A. Macchi *et al.*, Phys. Rev. Lett. **94**, 165003 (2005).
[9] A. Zhidkov *et al.*, Phys. Rev. Lett. **89**, 215002 (2002).
[10] L. O. Silva *et al.*, Phys. Rev. Lett. **92**, 015002 (2004).
[11] T. Zh. Esirkepov *et al.*, Phys. Rev. Lett. **92**, 175003 (2004).
[12] T. Zh. Esirkepov *et al.*, Phys. Rev. Lett. **96**, 105001 (2006).
[13] R. Benattar *et al.*, Rev. Sci. Instrum. **50**, 1583 (1979).
[14] L. A. Gizzi *et al.*, Phys. Rev. E **49**, 5628 (1994).
[15] T. Cowan *et al.*, Phys. Rev. Lett. **92**, 204801 (2004).
[16] E. Brambrink *et al.*, Phys. Rev. Lett. **96**, 154801 (2006).
[17] P. McKenna *et al.*, Phys. Rev. Lett. **98**, 145001 (2007).
[18] S. V. Bulanov *et al.*, Nucl. Instrum. Methods Phys. Res., Sect. A **540**, 25 (2005).
[19] H. Habara *et al.*, Phys. Rev. E **70**, 046414 (2004).
[20] J. Denavit, Phys. Rev. Lett. **69**, 3052 (1992).
[21] A. J. Mackinnon *et al.*, Phys. Rev. Lett. **86**, 1769 (2001).
[22] G. J. Pert, J. Comput. Phys. **43**, 111 (1981).
[23] T. Zh. Esirkepov, Comput. Phys. Commun. **135**, 144 (2001).
[24] M. Borghesi *et al.*, Phys. Rev. Lett. **81**, 112 (1998).